Progress In Electromagnetics Research, Vol. 130, 67–84, 2012

A NOVEL MULTIPORT MATCHING METHOD FOR MAXIMUM CAPACITY OF AN INDOOR MIMO SYSTEM

X. H. Yu[1], L. Wang[1], H. G. Wang[1, *], X. D. Wu[1], and Y. H. Shang[2]

[1]Department of Information Science & Electronic Engineering, Zhejiang University, Hangzhou 310027, China

[2]Department of Aeronautics and Astronautics, Zhejiang University, Hangzhou 310027, China

Abstract—A novel multiport matching method is devised to directly maximize the mean capacity with rigorous consideration of the mutual coupling effects of the matching network. In the RF front end of the real communication circuits, the mutual couplings always exist. In this paper, 1) a theoretical capacity upper bound of the 2-by-2 MIMO system with a matching network using the water-filling as the power allocation rule is analytically derived for the first time, 2) the Genetic Algorithm is employed to optimize the parameters of the matching network for the maximization of the mean capacity, 3) a coupled microstrip lines structure is devised to implement the matching network of the real MIMO receiving circuits by this matching method. The numerical results in the last section demonstrate that an optimized matching network obtained using our novel MPM method is capable to enhance the performance of the MIMO systems in a range of different indoor environments. This verifies that our method is not only effective but also practical.

1. INTRODUCTION

Recent researches [1, 2] show that MIMO system can provide substantial improvement in system capacity compared with the traditional SISO communication systems. In the physical layer, the MIMO channel includes four parts, viz., sources, loads, antennas and wireless multipath environment. All of them impact the performance

Received 6 April 2012, Accepted 1 July 2012, Scheduled 18 July 2012

* Corresponding author: Hao Gang Wang (hgwang@zju.edu.cn).

of a MIMO system. For a fixed two point communication, to enhance the capacity, one may either design a more fascinating MIMO antenna array to produce more multipath components and increase the receiving gain with lower transmitter and receiver correlations or match the impedance between feed lines and antennas [2]. In this paper, our study focuses on the second way for capacity enhancement, viz., the impedance matching. The matching network can be viewed as the fifth part of a MIMO system in the physical layer and plays an important role in improving the performance of a MIMO system.

Many researchers have studied the matching network to enhance the performance of a MIMO system. There are four conventional matching methods, viz., 1) 50 ohms match, 2) self-conjugate match, 3) multiport conjugate match [1] and 4) single port match [2, 3]. The first one sets the load impedance as 50 ohms, which equals to the characteristic impedance. The second one sets the load impedances as the conjugates impedances of the corresponding receiving antennas, the third one sets the impedance matrix of the matching network as the conjugate of antennas' impedance matrix and consider the mutual couplings of the matching network, while the last one optimize the impedances of transmission lines between receivers and loads, but it does not take into account the mutual couplings of the matching network existing practically. Methods 1), 2) and 3) are used to maximize the power but not necessarily to obtain maximum MIMO capacity. However, 4) maximizes the MIMO capacity, but it does not take into account the mutual couplings of the matching network connecting the receivers and loads.

In this manuscript, we derived a novel multiport matching method (MPM) for maximum mean capacity of an indoor MIMO system. The multiport matching method takes into account the mutual couplings between the transmission lines that connect the receive antennas and the loads. However, the conventional single port matching method [2, 3] neglects these mutual couplings of the matching network that always exist on the RF front end. The impedance matrix of this multiport matching network is not the conjugate impedance matrix of antenna array and is different with the multiport conjugate match [1]. Moreover, a theoretical derivation of capacity upper bound of the 2-by-2 MIMO system with a matching network using water-filling as a power allocation rule is presented. For validity of this MPM, we devised the coupled lines as a matching network and optimized the parameters by using GA as a nonlinear method for seeking the maximum mean capacity.

In this paper, a MIMO system with a matching network described by the admittance matrices is modeled in Section 2. The channel

model not only considers the mutual couplings of antennas on the transmitters and receivers but also the mutual couplings between the matching network that connects the receiver antennas and the loads. Section 3 presents a theoretical derivation of the capacity upper bound of a 2-by-2 MIMO system with a matching network. [4] has similar researches on the upper bound with the formula of capacity not taking account of water-filling. Moreover, only the impedance matrix for maximum capacity is provided without given a real structure in [4]. Instead, we derived the upper bound capacity of the 2-by-2 MIMO system with a matching network by the process that water-filling is described as the analytic formulas, viz., Equations (13) and (21) in Section 3. The process of the Genetic Algorithm (GA) [5] optimization is described in detail in Section 4. Section 5 introduces the test rooms, antennas array and the numerical results. In addition, this section gives a 2-by-2 MIMO system with a coupled microstrip transmission lines structure as the matching network. Finally, we also verify the admittance matrix of the coupled microstrip lines structure using the commercial electromagnetic full-wave softwares, viz., HFSS and IE3D.

Throughout this paper, the symbols $\bar{\bar{\bullet}}$ and $\bar{\bullet}$ denote a matrix and a vector respectively. $\bar{\bar{\bullet}}^{\dagger}$ denotes the Hermitian transpose of a matrix, $\det[\bar{\bar{\bullet}}]$ and $Tr[\bar{\bar{\bullet}}]$ are the determinant and the trace of a matrix.

2. MIMO CHANNEL MODEL

The MIMO system with a matching network can be equivalent to a microwave network as shown in Fig. 1. The model includes five parts, viz., sources, loads, antennas, matching network and wireless multipath environment. In Fig. 1, the RF circuits of loads and sources have been simplified as resistances of 50 ohms and voltage sources respectively.

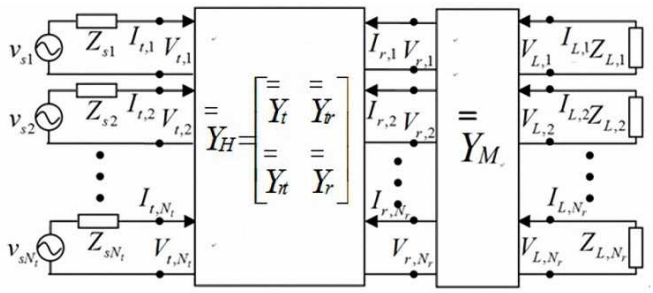

Figure 1. The equivalent circuit of a MIMO system with a matching network.

$\bar{\bar{Y}}_H$ is the admittance matrix of the propagation channel between transmitters and receivers. The relation between currents and voltages on transmitters and receivers is expressed as

$$\begin{bmatrix} \bar{I}_t^T \\ \bar{I}_r^T \end{bmatrix} = \bar{\bar{Y}}_H \cdot \begin{bmatrix} \bar{V}_t^T \\ \bar{V}_r^T \end{bmatrix} = \begin{bmatrix} \bar{\bar{Y}}_t & \bar{\bar{Y}}_{tr} \\ \bar{\bar{Y}}_{rt} & \bar{\bar{Y}}_r \end{bmatrix} \cdot \begin{bmatrix} \bar{V}_t^T \\ \bar{V}_r^T \end{bmatrix} \tag{1}$$

$\bar{\bar{Y}}_M$ is the admittance matrix of the matching network connecting the receivers and loads. It can be written as

$$\bar{\bar{Y}}_M = \begin{bmatrix} \bar{\bar{Y}}_{11} & \bar{\bar{Y}}_{12} \\ \bar{\bar{Y}}_{21} & \bar{\bar{Y}}_{22} \end{bmatrix} \tag{2}$$

where $\bar{\bar{Y}}_{11}$ and $\bar{\bar{Y}}_{22}$ denote the admittance matrices on the input ports and the output ports of the matching network, $\bar{\bar{Y}}_{12}$ and $\bar{\bar{Y}}_{21}$ represent the admittance matrices from the input ports to the output ports and from the output ports to the input ports. The relations between currents and voltages on receivers and loads are expressed as

$$\begin{bmatrix} -\bar{I}_r^T \\ \bar{I}_L^T \end{bmatrix} = \bar{\bar{Y}}_M \cdot \begin{bmatrix} \bar{V}_r^T \\ \bar{V}_L^T \end{bmatrix} = \begin{bmatrix} \bar{\bar{Y}}_{11} & \bar{\bar{Y}}_{12} \\ \bar{\bar{Y}}_{21} & \bar{\bar{Y}}_{22} \end{bmatrix} \cdot \begin{bmatrix} \bar{V}_r^T \\ \bar{V}_L^T \end{bmatrix} \tag{3}$$

$$\bar{\bar{Y}}_s \cdot \bar{V}_s = \bar{\bar{Y}}_s \cdot \bar{V}_t + \bar{I}_t \tag{4}$$

$$\bar{\mathbf{0}} = \bar{\bar{Y}}_L \cdot \bar{V}_L + \bar{I}_L \tag{5}$$

Because the feedback from the receivers to the transmitters can be ignored, the approximation (6) is employed.

$$\bar{I}_t \approx \bar{\bar{Y}}_t \cdot \bar{V}_t \tag{6}$$

where $\bar{I}_t = [I_{t,1} \ \ldots \ I_{t,N_t}]^T$, $\bar{I}_r = [I_{r,1} \ \ldots \ I_{r,N_r}]^T$ and $\bar{I}_L = [I_{L,1} \ \ldots \ I_{L,N_r}]^T$ denote the vectors of currents on transmitters, receivers and loads, $\bar{V}_s = [V_{s,1} \ \ldots \ V_{s,N_s}]^T$, $\bar{V}_t = [V_{t,1} \ \ldots \ V_{t,N_t}]^T$, $\bar{V}_r = [V_{r,1} \ \ldots \ V_{r,N_r}]^T$ and $\bar{V}_L = [V_{L,1} \ \ldots \ V_{L,N_r}]^T$ denote the vectors of voltages on sources, transmitters, receivers and loads, $\bar{\bar{Y}}_s = \mathrm{Diag}(Y_{s,1} \ \ldots \ Y_{s,N_t})$ and $\bar{\bar{Y}}_L = \mathrm{Diag}(Y_{L,1} \ \ldots \ Y_{L,N_r})$ denote the diagonal admittance matrix of the sources and loads. $\bar{\bar{Y}}_t$ and $\bar{\bar{Y}}_r$ are the input admittance matrices on transmitters and receivers respectively, while $\bar{\bar{Y}}_{rt}$ is the admittance matrix from input ports of transmitters to output ports of receivers and $\bar{\bar{Y}}_{tr}$ is from output ports of receivers to input ports of transmitters. Solving Equations (1)–(6), the relation between $\bar{V}_L$ and $\bar{V}_s$ can be written as

$$\begin{aligned} \bar{V}_L = & \left(\bar{\bar{Y}}_L + \bar{\bar{Y}}_{22}\right)^{-1} \cdot \bar{\bar{Y}}_{21} \cdot \left(\bar{\bar{Y}}_r + \bar{\bar{Y}}_{11} - \bar{\bar{Y}}_{12} \cdot \left(\bar{\bar{Y}}_L + \bar{\bar{Y}}_{22}\right)^{-1} \cdot \bar{\bar{Y}}_{21}\right)^{-1} \\ & \cdot \bar{\bar{Y}}_{rt} \cdot \left(\bar{\bar{Y}}_s + \bar{\bar{Y}}_t\right)^{-1} \cdot \bar{\bar{Y}}_s \cdot \bar{V}_s \end{aligned} \tag{7}$$

Thus, the single frequency MIMO channel matrix can be described as

$$\bar{\bar{H}} = \left(\bar{\bar{Y}}_L + \bar{\bar{Y}}_{22}\right)^{-1} \cdot \bar{\bar{Y}}_{21} \cdot \left(\bar{\bar{Y}}_r + \bar{\bar{Y}}_{11} - \bar{\bar{Y}}_{12} \cdot \left(\bar{\bar{Y}}_L + \bar{\bar{Y}}_{22}\right)^{-1} \cdot \bar{\bar{Y}}_{21}\right)^{-1} \cdot \bar{\bar{Y}}_{rt} \cdot \left(\bar{\bar{Y}}_s + \bar{\bar{Y}}_t\right)^{-1} \cdot \bar{\bar{Y}}_s \quad (8)$$

To use the channel model, $\bar{\bar{Y}}_t$, $\bar{\bar{Y}}_r$ in (8) and radiation patterns of transmitting and receiving antenna array are calculated using the multilevel Green's function interpolation method (MLGFIM) in [6–8], while the admittance matrix $\bar{\bar{Y}}_{rt}$ in (8) describing the interaction between the transmitting array and the receiving array is calculated using the method derived in [6] in which a ray tracing method is employed. Here a brief introduction of the MLGFIM and ray tracing technique is given. MLGFIM is an acceleration algorithm of the Method of Moments (MoM) and has a computational efficiency of $O(N \log N)$ for solving the electric middle size EM problems while the conventional MoM has a computational efficiency of $O\left(N^2\right)$. The N is the number of unknowns.

To launch the ray tracings [9–12], we combine using the brute force method (or pincushion method) and the image method [13]. A spherical bunch of evenly distributed rays with $\Delta\Omega$ solid angle separation are incident from the reference center of the transmitter array. These rays then propagate straightforwardly if no obstruction is encountered. If the ray (named ray A here) is intersect with a wall, the reflection point is located and this ray will reflect from the reflection point and propagate straightforwardly again. Here we set a cube whose center is just the reference center of the receiving array. If ray A will hit the cube, there may be a ray that starts from the reference center of the transmitter and finally hit the reference center of the receiver. This ray will intersect with and reflect from all the walls that ray A does before it reach the cube. Because we have found the walls that this ray intersect with, we can easily find its exact path using the image method. We also compare this ray with the rays we have found to ensure that it is a new found one. In our program, we also consider the transmission of the rays by just taking into account TE and TM transmittances of the very thin (whose thickness is greatly less than one wavelength) layered dielectric structures. In the ray tracing procedure, the maximum number of reflections of a ray, the length of the cube, and the solid angle are 15, 0.8 meters, and 0.25 square degrees, respectively.

3. THEORETICAL DERIVATION

In this section, we derive a theoretic capacity upper bound of a 2-by-2 MIMO system. Equation (25) in Appendix A is commonly used to calculate the capacity of a MIMO system [14]. The recent study [15] has shown that if $\mu > \lambda_i^{-1}$ using water-filling, the maximum capacity is obtained when the condition number of the matrix $\bar{\bar{H}}^{\dagger} \cdot \bar{\bar{H}}$ is minimum. Thus, (25) and (32) can be rewritten as

$$C_{\text{apacity}} = \log_2 \left(\left(\frac{SNR + \sum_{i=1}^{N_t} \lambda_{ni}^{-1}}{N_t} \right)^{N_t} \cdot \prod_{i=1}^{N_t} \lambda_{ni} \right) \tag{9}$$

The constraint is

$$\sum_{i=1}^{N_t - 1} \left(\lambda_{nN_t}^{-1} - \lambda_{ni}^{-1} \right) \leq SNR \tag{10}$$

where it is assumed that $\lambda_{n1} > \lambda_{n2} \ldots > \lambda_{nN_t}$. For maximum capacity, (10) is the power restriction condition, λ_{ni} are the eigenvalues of $\bar{\bar{H}}_n^{\dagger} \cdot \bar{\bar{H}}_n$ where $\bar{\bar{H}}_n$ and $\bar{\bar{H}}_n^{\dagger}$ is the normalization of $\bar{\bar{H}}$ and $\bar{\bar{H}}^{\dagger}$. And they can be represented by λ_i which are the eigenvalues of $\bar{\bar{H}}^{\dagger} \cdot \bar{\bar{H}}$.

$$\bar{\bar{H}}_n = \frac{\bar{\bar{H}}}{N_{\text{or}}} = \left(\frac{\sum_{i=1}^{k} \sum_{j=1}^{k} |h_{ij}|^2}{N_t N_r} \right)^{-\frac{1}{2}} \bar{\bar{H}} = \left(\frac{Tr\left[\bar{\bar{H}} \cdot \bar{\bar{H}}^{\dagger} \right]}{N_t N_r} \right)^{-\frac{1}{2}} \bar{\bar{H}} \tag{11}$$

$$\lambda_{ni} = \frac{\lambda_i}{N_{or}^2}, \quad i = 1, \ldots, N_t \tag{12}$$

h_{ij} in (11) is the entry in i-th row and the j-th column of $\bar{\bar{H}}$. In this paper, a 2-by-2 MIMO system is taken as an example. Thus, (9) and (10) are rewritten respectively as (13) and (14).

$$\begin{aligned} C_{apacity} &= \log_2 \left(\left(\frac{SNR + \lambda_{n1}^{-1} + \lambda_{n2}^{-1}}{2} \right)^2 \lambda_{n1} \lambda_{n2} \right) \\ &= \log_2 \left(SNR^2 \cdot \frac{4\lambda_1 \lambda_2}{(\lambda_1 + \lambda_2)^2} + \frac{(\lambda_1 + \lambda_2)^2}{4\lambda_1 \lambda_2} + 2SNR \right) \\ &= \log_2 \left(SNR^2 \cdot W + W^{-1} + 2SNR \right) \end{aligned} \tag{13}$$

$$\lambda_{n2}^{-1} - \lambda_{n1}^{-1} = \frac{\sqrt{1 - W}}{W} \leq SNR \tag{14}$$

For convenience, it's assumed that

$$W = \frac{4\lambda_1\lambda_2}{(\lambda_1+\lambda_2)^2} = \frac{4\det\left[\bar{\bar{H}}^\dagger \cdot \bar{\bar{H}}\right]}{\left(Tr\left[\bar{\bar{H}}^\dagger \cdot \bar{\bar{H}}\right]\right)^2} \tag{15}$$

To get the maximum capacity, (14) is the necessary condition and the solution is

$$W_1 \le W \le 1, \quad W_1 = \frac{\sqrt{1+4SNR^2}-1}{2SNR^2} \tag{16}$$

For power, it is assumed that the matching network is lossless, so all the elements of $\bar{\bar{Y}}_M$ are pure imaginary. Considering the reciprocity and geometric symmetry of the matching network structure, e.g., a coupled microstrip lines structure [16], $\bar{\bar{Y}}_M$ can be simplified as (24) in Section 4. Thus, by substituting (31)–(35) into (15), we can obtain Equation (17).

$$W = \frac{4\det\left[\bar{\bar{H}}^\dagger \cdot \bar{\bar{H}}\right]}{\left(Tr\left[\bar{\bar{H}}^\dagger \cdot \bar{\bar{H}}\right]\right)^2} = \frac{4k_3\left(U^2-V^2\right)}{\left(k_1U+k_2V\right)^2} = \frac{4k_3\left(1-K^2\right)}{\left(k_1+k_2K\right)^2}, \quad K = \frac{V}{U} \tag{17}$$

The solution of (17) is

$$K = \frac{-k_1k_2W \pm 2\sqrt{4k_3^2 - k_3W\left(k_1^2-k_2^2\right)}}{Wk_2^2+4k_3} \tag{18}$$

According to the definitions of k_1, k_2 and k_3 in Appendix B, the inequalities in (19) can be derived.

$$k_1+k_2>0, \quad k_1-k_2>0, \quad k_3>0 \tag{19}$$

$$\Delta = 4k_3^2 - k_3W\left(k_1^2-k_2^2\right) \ge 0 \Rightarrow W \le W_2, \quad W_2 = \frac{4k_3}{k_1^2-k_2^2} \tag{20}$$

For a practical system, solution must exist, so (20) must be required. According to (16) and (20), the Winterval is $[W_1,1]\cap(0,W_2]$. There is no solution for W when $W_1 > W_2$. Thus, the Equation (25) in Appendix B can be simplified as

$$\begin{aligned} C_{\text{apacity}} &= \log_2(SNR*\lambda_{n2}+1) \\ &= \log_2(SNR*4*\lambda_2/(\lambda_1+\lambda_2)+1) < \log_2(4SNR+1) \end{aligned} \tag{21}$$

We define function $F_{(W)}$ in (22) for convenience when $W_1 \le W_2$, which has the same monotonic property with the capacity in (13).

$$F_{(W)} = SNR^2\cdot W + W^{-1} + 2SNR, \ W \in [W_1,1]\cap(0,W_2] \text{ and } W_1 \le W_2. \tag{22}$$

According to the monotonic property, the maximum locates on the bound of the W interval. The lower and upper bound are W_1 and $\min(W_2, 1)$ respectively. Thus, the maximum value of F can be written as

$$F_{(W)\max} = \max\{F(\min(W_2, 1)), F(W_1)\} \tag{23}$$

According to (21) and (23), the upper bound can be obtained.

The derivation above is only for a transmitter-receiver pair. It can be used as an upper bound of the MIMO capacity. However, in this paper, we also need to maximize the mean capacity indoor where receivers distribute in a region. This maximization procedure is a nonlinear problem and is too complicated to be accomplished by using analytical method discussed in this section. Thus, we need to use the nonlinear optimization algorithm. According to the "no lunch free theorem" described in [17], all optimization algorithms have the same performance when averaged over all possible cost functions but with different performances for a special problem.

4. OPTIMIZATION USING GA

The heuristics methods, e.g., GA [5] and Simulated Annealing (SA) [18], can effectively avoid the local optimal solution while the traditional nonlinear methods, e.g., conjugate gradient method, Newton method and gradient descent, cannot. The GA and SA are suit for the high dimension solution space (HDSS) and low dimension solution space (LDSS) respectively [19]. The dimension solution space becomes higher when the number of MIMO antennas increases. Thus, GA is used as a nonlinear method to optimize the admittance matrix of a matching network in this paper, while SA is used to check the accuracy of optimized results with GA. GA is a heuristic algorithm that mimics the process of natural evolution introduced in [5], i.e., inheritance, mutation, selection and crossover, to seeking maximum or minimum. For a problem, GA requires chromosomes and a fitness function to evaluate the solution. The genes of chromosomes usually are the unknowns of the problem. The fitness function is the target variable which is the maximum or minimum in special scopes of unknowns. Generally, the size of population and generation, probability of mutation and probability of crossover can be adjusted for the accuracy and efficiency of GA.

GA is used to optimize antennas array in [20, 21]. In this manuscript, we assume that the matching network is lossless with the assumption of reciprocity and geometric symmetry of the structure, so the admittance matrix can be rewritten as Equation (24). For the

optimization of a 2-by-2 MIMO system with MPM, elements of $\bar{\bar{Y}}_M$ in (24) and formula (25) are set as the genes of chromosomes and the fitness function of GA, respectively.

$$\bar{\bar{Y}}_M = \begin{bmatrix} \bar{\bar{Y}}_{11} & \bar{\bar{Y}}_{12} \\ \bar{\bar{Y}}_{21} & \bar{\bar{Y}}_{22} \end{bmatrix} = j \begin{bmatrix} s_1 & m_1 & s_2 & m_2 \\ m_1 & s_1 & m_2 & s_2 \\ s_2 & m_2 & s_1 & m_1 \\ m_2 & s_2 & m_1 & s_1 \end{bmatrix} \tag{24}$$

where s_1, s_2, m_1 and m_2 are pure real for the matching network is lossless.

Because (24) describes the admittance matrix of an unfixed matching network, it can be lossless with the assumption of reciprocal and symmetrical structure. Thus, considering a practical matching network, its structure is fixed and the $\bar{\bar{Y}}_M$ can be described by the geometric parameters of this structure. For instance, a coupled microstrip lines structure is commonly used in projects. We can use the coupled microstrip analytical method (CMAM) to describe the relations between the admittance matrix and geometric parameters [22, 23]. The admittance matrix of a coupled microstrip figured in Fig. 2 can be represented by s_1, m_1, s_2 and m_2 which can be calculated by the formulas (5a)–(5d) in literature [22] where Y_{0e} and Y_{0o} are the even and odd mode characteristic admittances, θ_e and θ_o are the even and odd mode electrical lengths of the lines. [22, 23] show that these four parameters are related with the normalization gap (s/h), the normalization width (w/h) and the physical length (L) of a coupled microstrip lines structure in Fig. 2. Thus, we set these three parameters as the genes of chromosomes. In our simulation, the height and relative permittivity of the substrate are set to 0.001 meter and 4.4, respectively. The procedure that the GA used to maximize the mean capacity of an indoor MIMO system is introduced in Table 1.

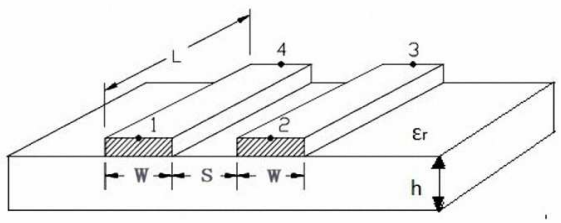

Figure 2. A simple symmetric structure of a coupled microstrip.

Table 1. The procedure of the novel MPM method with GA.

1. Calculate the admittances $\bar{\bar{Y}}_r$, $\bar{\bar{Y}}_t$ and radiation pattern of the antennas array with MLGFIM in [6, 7, 24];
2. Calculate the path losses of all the paths from a transmitter to a receiver with ray tracing method in the test room listed in Fig. 3, then get the $\bar{\bar{Y}}_{rt}$ in [6];
3. Optimize $\bar{\bar{Y}}_M$ with GA: initialize the size of population and generation, probability of mutation and probability of crossover; set the geometric parameters, viz., the normalization width, the normalization gap and the length, relating with the admittance matrix as the genes of chromosomes, then set (25) listed in the Appendix A as the fitness function;
4. Compare the optimal results with the mean capacities of the MIMO system without a matching network;
5. To verify the numerical results of step 3, we simulate the structure with the optimal solution by the electromagnetic fullwave softwares, viz., HFSS and IE3D.

5. NUMERICAL ANALYSIS

Throughout the paper, the working frequency is 1.969 GHz, *SNR* is 20 dB.

5.1. The Test Antennas and Test Rooms

The antennas are introduced in [6, 24, 25]. The planar array shown in Fig. 6 in [6] is used as the transmitters and receivers of a 2-by-2 MIMO system. The radius and height of the monopoles are 0.00118 m and 0.0358 m, respectively, the gap radius is 0.00262 m and the finite ground is square of 0.4 m $\times$ 0.4 m. We calculate the impedance of the array with MLGFIM in [6, 7]. Fig. 10 in [6] shows the self and mutual impedances with the various spacing between the two monopoles.

One test room is figured in Fig. 3. In the room, there are two desks, two chairs and one barrier between them whose coordinates are

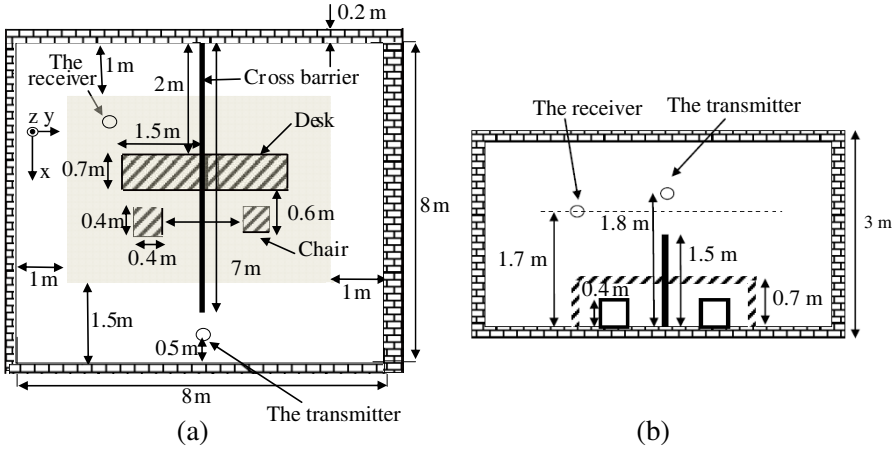

Figure 3. A closed room with two desks, two chairs (dashed area) and one barrier (solid bold line). (a) Top view. (b) Side view.

denoted in Fig. 3. Here, we 1) apply our newly developed MLGFIM to calculate the mutual admittance matrices and the radiation patterns of the transmitter and receiver; 2) use the brute-force method and ray tracing method with at most 15 reflections to search the paths from the transmitter to the receiver. Also, it is assumed that 1) the walls of the room are built up with 20 cm thick material. The ceiling and the barrier of the room is the metal plates that can be approximated to be PEC; 3) the ground of the room has a high dielectric constant and is also approximated to be PEC. For mean MIMO capacity, we have 50*50 samples of receivers in shadow listed in Fig. 3 with Monte Carlo method.

For the validation of the optimization, we simulated the mean capacity with the same matching network in the other test rooms listed in Table 2. The gray areas shown in Fig. 3(a) is the sampling area. Its size is invariant if the size of the room is unchanged. While the size of the room increases the gray area also increases. However the sampling density and the distances between the edges of the gray area and the walls keep constant. The transmitter is fixed on the point $(l - \Delta, l/2, 1.8\,\mathrm{m})$ where l is the width of the room and Δ is the distance between the transmitter and the nearest wall. Here we set Δ to 0.5 meter. Comparing with the layout of room 1 listed in Fig. 3, the facilities in room one are removed. Comparing with room 2, the size of room 3 is different. Comparing with room 2, the medium of the wall of room 4 is different.

Table 2. The test rooms.

No.	Size (m)	Characteristic	No.	Size	Characteristic
1	8*8*3	four brick walls, a cross barrier, two desks and two chairs	3	10*10*3	four brick walls without barrier
2	8*8*3	four brick walls without barrier	4	8*8*3	four casement walls without barrier

Table 3. The numerical results obtained by GA.

spacing	**0.05**	**0.10**	**0.15**	**0.20**	**0.25**	**0.30**	**0.35**	**0.40**	**0.45**	**0.50**
w/h	9.99	9.92	9.86	9.79	9.46	1.06	1.06	1.01	1.01	1.10
s/h	7.10	9.97	8.19	9.86	9.62	1.12	1.10	1.10	1.21	1.14
L	19.85	19.91	19.93	19.89	19.98	12.64	15.07	15.07	19.56	15.94

The units of spacing between antennas and length of the coupled lines are wavelength and millimeter

5.2. The Design and Verification of a Coupled Microstrip

Throughout this paper, while using GA, 1) the size of population and generation are chosen to 100 and 50; 2) the probability of mutation and probability of crossover are 0.4 and 0.6 respectively. The three parameters, viz., the normalization gap (s/h), normalization width (w/h) and the physical length (L), are set as the genes of chromosomes and their domains are (1, 10), (1, 10) and (5, 20) millimetres, respectively.

To check if the results of GA are maximal, SA is used to be compared with GA in Fig. 4 of Subsection 5.3. After obtaining the optimal geometric parameters using GA, we need to verify them using the fullwave EM simulation tools. We used these geometric parameters to calculate the admittance matrix by CMAM, HFSS and IE3D to show that GA results are correct. Finally, we substituting the admittance matrices into (8) and calculate the capacity with (25) in Appendix A to verify the structure.

5.3. Numerical Results

The optimization solutions of the coupled microstrip lines using GA are listed in Table 3 and the admittance matrices calculated by CMAM, HFSS and IE3D using the data in Table 3 are listed in Table 4. It's shown that the values of the matrices obtained using

Table 4. The four elements of the admittance matrices of the coupled microstrip with CMAM, HFSS and IE3D.

	spacing	Y_{11} (mS)	Y_{12} (mS)	Y_{13} (mS)	Y_{14} (mS)	spacing	Y_{11} (mS)	Y_{12} (mS)	Y_{13} (mS)	Y_{14} (mS)
CMAM		3.3174	0.5603	−0.7544	68.0092		3.5580	0.3223	−0.5343	67.7413
HFSS	0.05	4.7738	0.2885	−0.5848	68.1047	0.10	4.9811	0.0940	−0.3623	67.6288
IE3D		3.3510	0.7416	−0.8891	67.0200		3.5890	0.4932	−0.6220	66.6400
CMAM		3.6583	0.4464	−0.6411	67.3409		3.3412	0.3280	−0.5303	66.9579
HFSS	0.15	5.1275	0.1807	−0.4888	67.3207	0.20	4.7638	0.0837	−0.3684	66.8999
IE3D		3.6850	0.6229	−0.7612	66.3100		3.3770	0.4953	−0.6231	65.8700
CMAM		3.6010	0.3379	−0.5161	65.0929		−11.2175	2.2593	−2.8599	18.5719
HFSS	0.25	4.9334	0.1036	−0.3733	65.0585	0.30	−10.7815	2.6222	−3.1482	18.6443
IE3D		3.6230	0.4968	−0.6204	64.0400		−11.0300	2.1980	−2.7730	18.3100
CMAM		−7.5412	1.7815	−2.5171	16.6234		−8.0664	1.6590	−2.2321	16.4707
HFSS	0.35	−7 1177	2.0563	−2.7272	16.8984	0.40	−6.9998	2.0376	−2.6815	16.4840
IE3D		−7.4270	1.7440	−2.4480	16.4200		−7.9160	1.6190	−2.1650	16.2400
CMAM		−2.0875	1.0422	−1.8392	14.5578		−6.4526	1.6112	−2.3537	16.3594
HFSS	0.45	−1 6190	1.2843	−1.9087	15.0849	0.50	−6.0115	1.8618	−2.5128	16.6523
IE3D		−2 0480	1.0330	−1.7910	14.3900		−6.3930	1.5890	−2.2990	16.1900

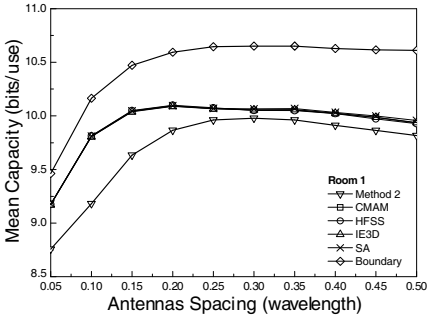

Figure 4. The mean capacities when the admittance matrix is calculated by CMAM, HFSS and IE3D with the same optimal solution.

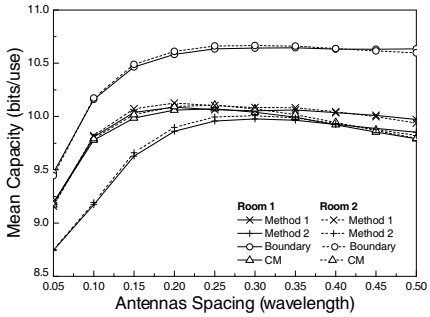

Figure 5. The mean capacities of the 2-by-2 MIMO system in the rooms with the same size and medium of walls but different layouts.

these three different EM methods agree very well. Moreover, the mean capacities of the 2-by-2 MIMO system in Fig. 4, which are calculated by substituting the admittance matrices into (8) respectively, nearly have the same performance. The results of GA and SA are nearly the same. It's shown that the design which uses a coupled microstrip as a matching network is valid.

We use the optimization solutions to simulate mean capacity of the 2-by-2 MIMO system for all rooms in Table 1 to show the performance of our MPM. In the figures from 4 to 6, 1) Method 1 is that the matching network is fixed for all rooms; 2) Method 2 is that the MIMO

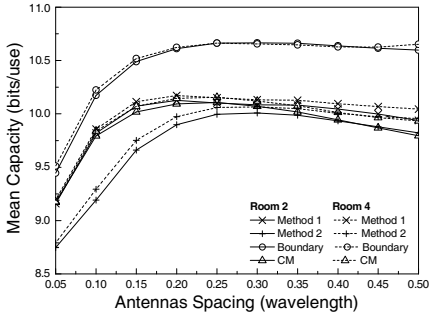

Figure 6. The mean capacities of the 2-by-2 MIMO system in the rooms with the same size and layout but different medium of walls.

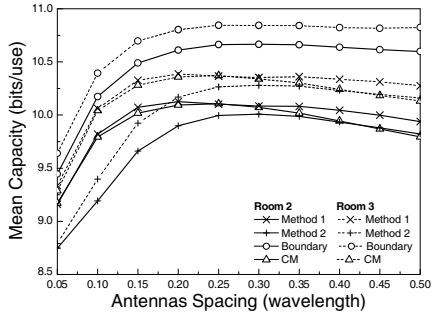

Figure 7. The mean capacities of the 2-by-2 MIMO system in the rooms with the same layout and medium of walls but different size.

system has no matching network; 3) the boundary is the average value of the theoretical maximum capacity upper bounds of all transmitter-receiver pairs when the receivers locate at different sampled points of the gray area; 4) the CM represents the self-conjugate match method.

We test a 2-by-2 MIMO system with the fixed optimized matching network obtained using our novel MPM method in a range of different indoor environments. Figs. 5, 6 and 7 show the mean capacities of the matched MIMO systems for the rooms with different layouts, different mediums of the walls and different sizes, respectively. We see that the performances of the matched MIMO systems for the rooms with different layouts are similar, while the performances for the rooms with different mediums of the walls or different sizes are different. More importantly, the results in Figs. 5, 6 and 7 also show that a fixed optimized matching network obtained using our novel MPM method is capable to enhance the performance of the MIMO systems in a range of different indoor environments.

6. CONCLUSION

This paper presents a novel optimal multiport matching network for the maximum mean capacity of a 2-by-2 MIMO system. The novel MPM method takes into account the mutual couplings neglected by the single port matching method for the maximum mean capacity. Moreover, a theoretical capacity upper bound using water-filling as the power allocation is derived for the first time in Section 3. According to the numerical results, the optimum mean capacities with the MPM network are significantly better than the mean capacities without a

matching network. The 2-by-2 MIMO systems with the fixed matching network have better performance than the MIMO systems without matching network in the rooms with different layouts, different medium of walls or different sizes. Good agreements are observed between the admittance matrices in Table 4 obtained by CMAM and the two full-wave EM tools, viz., HFSS and IE3D. Moreover, the mean capacities corresponding to these admittance matrices are coincident with each other. This further verifies our novel MPM method.

ACKNOWLEDGMENT

This work is supported by the National Natural Science Foundation of China No. 60971056, and National High Technology "863" Programs of China under Grant No. 2009AA01Z226.

APPENDIX A.

By using water-filling [14], the system capacity formula is expressed as

$$C = \sum_{i=1}^{N_t} (\log_2(\mu\lambda_i))^+ \tag{A1}$$

where a^+ denotes $\max\{0, a\}$; λ_i is the eigenvalues of $\bar{\bar{H}}^\dagger \cdot \bar{\bar{H}}$, ($\bar{\bar{H}}^\dagger$ the Hermitian of the channel matrix $\bar{\bar{H}}$); μ is chosen to meet the power constraint.

$$\sum_{i=1}^{N_t} \left(\mu - \lambda_i^{-1}\right)^+ = P/\sigma^2 = SNR \tag{A2}$$

APPENDIX B.

It is assumed that $\bar{\bar{H}} = \bar{\bar{Y}}_{h1} \cdot \bar{\bar{Y}}_{h2}$ for (8). Thus,

$$\bar{\bar{Y}}_{h1} = \left(\bar{\bar{Y}}_L + \bar{\bar{Y}}_{22}\right)^{-1} \cdot \bar{\bar{Y}}_{21} \cdot \left(\bar{\bar{Y}}_r + \bar{\bar{Y}}_{11} - \bar{\bar{Y}}_{12} \cdot \left(\bar{\bar{Y}}_L + \bar{\bar{Y}}_{22}\right)^{-1} \cdot \bar{\bar{Y}}_{21}\right)^{-1} \tag{B1}$$

$$\bar{\bar{Y}}_{h2} = \bar{\bar{Y}}_{rt} \cdot \left(\bar{\bar{Y}}_s + \bar{\bar{Y}}_t\right)^{-1} \cdot \bar{\bar{Y}}_s \tag{B2}$$

In this paper, all of $\bar{\bar{Y}}_r$, $\bar{\bar{Y}}_t$, $\bar{\bar{Y}}_L$, $\bar{\bar{Y}}_s$, $\bar{\bar{Y}}_{11}$, $\bar{\bar{Y}}_{12}$, $\bar{\bar{Y}}_{21}$ and $\bar{\bar{Y}}_{22}$ are 2×2 complex symmetric Toeplitz matrices [26], so $\bar{\bar{Y}}_{h1}$ also is a 2×2 complex symmetric Toeplitz matrix. Thus,

$$\bar{\bar{Y}}_{h1}^\dagger \cdot \bar{\bar{Y}}_{h1} = \begin{bmatrix} y_{h1,11} & y_{h1,12} \\ y_{h1,12} & y_{h1,11} \end{bmatrix}^\dagger \cdot \begin{bmatrix} y_{h1,11} & y_{h1,12} \\ y_{h1,12} & y_{h1,11} \end{bmatrix}$$

$$= \begin{bmatrix} \sum_{i=1}^{2} |y_{h1,1i}|^2 & 2\mathrm{Re}\left(y_{h1,11}^{\dagger} y_{h1,12}\right) \\ 2\mathrm{Re}\left(y_{h1,11}^{\dagger} y_{h1,12}\right) & \sum_{i=1}^{2} |y_{h1,1i}|^2 \end{bmatrix} = \begin{bmatrix} U & V \\ V & U \end{bmatrix} \quad \text{(B3)}$$

where $U > 0$, $V \neq 0$ and $U, V \in R$.

$$\begin{aligned} \bar{\bar{Y}}_{h4} &= \bar{\bar{Y}}_{h2} \cdot \bar{\bar{Y}}_{h2}^{\dagger} = \begin{bmatrix} y_{h2,11} & y_{h2,12} \\ y_{h2,21} & y_{h2,22} \end{bmatrix} \cdot \begin{bmatrix} y_{h2,11} & y_{h2,12} \\ y_{h2,21} & y_{h2,22} \end{bmatrix}^{\dagger} \\ &= \begin{bmatrix} \sum_{j=1}^{2} |y_{h2,1j}|^2 & \sum_{j=1}^{2} y_{h2,1j} y_{h2,2j}^{\dagger} \\ \sum_{j=1}^{2} y_{h2,2j} y_{h2,1j}^{\dagger} & \sum_{j=1}^{2} |y_{h2,2j}|^2 \end{bmatrix} \end{aligned} \quad \text{(B4)}$$

$$\begin{aligned} Tr\left[\bar{\bar{H}}^{\dagger} \cdot \bar{\bar{H}}\right] &= Tr\left[\bar{\bar{Y}}_{h2}^{\dagger} \cdot \bar{\bar{Y}}_{h1}^{\dagger} \cdot \bar{\bar{Y}}_{h1} \cdot \bar{\bar{Y}}_{h2}\right] = Tr\left[\underbrace{\bar{\bar{Y}}_{h2} \cdot \bar{\bar{Y}}_{h2}^{\dagger}}_{\bar{\bar{Y}}_{h4}} \cdot \underbrace{\bar{\bar{Y}}_{h1}^{\dagger} \cdot \bar{\bar{Y}}_{h1}}_{\bar{\bar{Y}}_{h3}}\right] \\ &= \sum_{i=j=1}^{2} y_{h4ij} \cdot U + \sum_{i=1}^{2} \sum_{j=1, j\neq i}^{2} y_{h4ij} \cdot V \end{aligned} \quad \text{(B5)}$$

$$\det\left[\bar{\bar{H}}^{\dagger} \cdot \bar{\bar{H}}\right] = \det\left[\bar{\bar{Y}}_{h4}\right]\left(U^2 - V^2\right) \quad \text{(B6)}$$

where we assume three parameters for convenience.

$$k_1 = \sum_{i=j=1}^{2} y_{h4ij} = \sum_{i=1}^{2}\sum_{j=1}^{2} |y_{h2,ij}|^2 \quad \text{(B7)}$$

$$k_2 = \sum_{i=1}^{2} \sum_{j=1, j\neq i}^{2} y_{h4ij} = 2\sum_{j=1}^{2} \mathrm{Re}\left(y_{h2,1j} y_{h2,2j}^{\dagger}\right) \quad \text{(B8)}$$

$$k_3 = \det\left[\bar{\bar{Y}}_{h4}\right] = \det\left[\bar{\bar{Y}}_{h2} \cdot \bar{\bar{Y}}_{h2}^{\dagger}\right] = \det\left[\bar{\bar{Y}}_{h2}\right] \det\left[\bar{\bar{Y}}_{h2}^{\dagger}\right] = \left|\det\left[\bar{\bar{Y}}_{h2}\right]\right|^2 \quad \text{(B9)}$$

REFERENCES

1. Wallace, J. W. and M. A. Jensen, "Mutual coupling in MIMO wireless systems: A rigorous network theory analysis," *IEEE Trans. on Wireless Commun.*, Vol. 3, No. 4, 1317–1325, Jul. 2004.
2. Lau, B. K., J. B. Anderson, G. Kristensson, and F. Molisch, "Impact of matching network on bandwidth of compact antenna arrays," *IEEE Trans. on Antennas and Propagat.*, Vol. 54, No. 11, 3225–3238, Nov. 2006.

3. Fei, Y., Y. Fan, B. K. Lau, and J. S. Thompson, "Optimal single-port matching impedance for capacity maximization in compact MIMO arrays," *IEEE Trans. on Antennas and Propagat.*, Vol. 56, No. 11, 3566–3575, Nov. 2008.
4. Tsen, W.-F. and H. J. Li, "Optimal impedance matching for capacity maximization of MIMO systems with coupled antennas and noisy amplifiers," *Progress In Electromagnetics Research C*, Vol. 15, 23–36, 2010.
5. Bagchi, T. P., *Multi Objective Scheduling by Genetic Algorithms*, 1999.
6. Wang, H. G. and L. Wang, "A novel numerical model for simulating three dimensional MIMO channels with complex antenna arrays," *IEEE Trans. on Antennas and Propagat.*, Vol. 57, No. 8, 2439–2451, Aug. 2009.
7. Wang, H. G. and C. H. Chan, "The implementation of multilevel Green's function interpolation method for full-wave electromagnetic problems," *IEEE Trans. on Antennas and Propagat.*, Vol. 55, No. 5, May 2007.
8. Shi, Y., X. Luan, J. Qin, C. Lv, and C.-H. Liang, "Multilevel Green's function interpolation method solution of volume/surface integral equation for mixed conducting/bi-isotropic objects," *Progress In Electromagnetics Research*, Vol. 107, 239–252, 2010.
9. Bertoni, H. L., *Radio Propagation for Modern Wireless Systems*, Prentice Hall, NJ, 2000.
10. Liu, Z.-Y. and L.-X. Guo, "A quasi three-dimensional ray tracing method based on the virtual source tree in urban microcellular environments," *Progress In Electromagnetics Research*, Vol. 118, 397–414, 2011.
11. Reza, W. A., M. S. Sarker, and K. Dimyati, "A novel integrated mathematical approach of ray-tracing and genetic algorithm for optimizing indoor wireless coverage," *Progress In Electromagnetics Research*, Vol. 110, 147–162, 2010.
12. Sarker, M. S., A. W. Reza, and K. Dimyati, "A novel ray-tracing technique for indoor radio signal prediction," *Journal of Electromagnetic Waves and Applications*, Vol. 25, Nos. 8–9, 1179–1190, 2011.
13. Chen, S.-H. and S.-K. Jeng, "An SBR/image approach for radio wave propagation in indoor environments with metallic furniture," *IEEE Trans. on Antennas and Propagat.*, Vol. 45, No. 1, 98–106, Jan. 1997.
14. Telatar, I. E., "Capacity of multi antenna Gaussian channels,"

AT&T Bell Labs. Internal Tech. Memo., Jun. 1995.

15. Chiurtu, N., B. Rimoldi, and E. Telatar, "On the capacity of multi-antenna gaussian channels," *IEEE International Symposium on Information Theory*, Washington, DC, Jun. 24–29, 2001.
16. Pozar, D. M., *Microwave Engineering*, 3rd Edition, 226–227, 2004.
17. Wolpert, D. H. and W. G. Macready, "No free lunch theorems for optimization," *IEEE Transactions on Evolutionary Computation*, Vol. 1, No. 1, 67–82, Apr. 1997.
18. Kirkpatrick, S., C. D. Gelatt, and M. P. Vecchi, "Optimization by simulated annealing," *Science*, Vol. 220, No. 4598, 671–680, 1983.
19. Fulginei, F. R. and A. Salvini, "Comparative analysis between modern heuristics and hybrid algorithms," *COMPEL: The International Journal for Computation and Mathematics in Electrical and Electronic Engineering*, Vol. 26, No. 2, 259–268, 2007.
20. Siakavara, K., "Novel fractal antenna arrays for satellite networks: Circular ring Sierpinski carpet arrays optimized by genetic algorithms," *Progress In Electromagnetics Research*, Vol. 103, 115–138, 2010.
21. Dadgarnia, A. and A. A. Heidari, "A fast systematic approach for microstrip antenna design and optimization using ANFIS and GA," *Journal of Electromagnetic Waves and Applications*, Vol. 24, No. 16, 2207–2221, 2010.
22. Gaorga, I. Z. and A. K. Johnson, "Coupled transmission line networks in an inhomogeneous dielectric medium," *IEEE Transactions on Microwave Theory and Techniques*, Vol. 17, No. 10, 753–750, Oct. 1969.
23. Kirschning, M. and R. H. Jansen, "Accurate wide-range design equations for the frequency-dependent characteristic of parallel coupled microstrip lines," *IEEE Transactions on Microwave Theory and Techniques*, Vol. 27, No. 1, 83–90, Jan. 1984.
24. Wang, L. and H. G. Wang, "An analytical three dimensional correlation model for array with antennas having arbitrarily oriented directions," *IEEE Asia Pacific Microwave Conference*, Hong Kong, Dec. 2008.
25. Wang, L. and H. G. Wang, "Regular polyhedron antenna array design and simulation for MIMO systems," *PIERS Proceedings*, 1487–1490, Beijing, China, Mar. 23–27, 2009.
26. Gray, R. M., *Toeplitz and Circulant Matrices: A Review*, 2006.